CrossMark

ORIGINAL PAPER

Characterization of an Air-Based Coaxial Dielectric Barrier Discharge Plasma Source for Biofilm Eradication

Juliana Soler-Arango[1] · Graciela Brelles-Mariño[1] · Antonio Rodero[2] ·
Maria C. Garcia[3] 🔟

Abstract Air-based atmospheric-pressure cold plasmas are a source of charged particles, excited species, radicals, and UV rays, known to induce degradation of biomaterials. In this work we characterize an air-based Dielectric Barrier Discharge plasma source designed for biofilm eradication, and study plasmas generated under different conditions by Optical Emission Spectroscopy. The main excited species in air-based plasmas are N_2 ($C^3\Pi_u$) molecules and the gas temperatures never exceed 335 K, decreasing as air amounts increase in the feeding gas. Excited oxygen atoms and OH species are only detected in discharges generated in argon-containing gases. The temperature of the effluent remains below 308 K. Air-based plasmas are useful for biofilm eradication as they produce high amounts of ozone at a low gas temperature.

Keywords Atmospheric plasmas · Biofilm eradication · Cold plasmas · Gas temperature · Optical emission spectroscopy

Introduction

In the two last decades, a significant progress in the design of innovative non-thermal plasma sources operating in the open atmosphere has taken place. Their easy handling, conferred by the atmospheric pressure condition, along with their ability to induce physical

✉ Maria C. Garcia
fa1gamam@uco.es

1 Center for Research and Development on Industrial Fermentations, Consejo Nacional de Investigaciones Científicas y Técnicas (CINDEFI, CCT-LA PLATA-CONICET), Facultad de Ciencias Exactas, Universidad Nacional de La Plata, La Plata, Argentina

2 Department of Physics, University of Cordoba, Ed- C2, Campus de Rabanales, 14071 Córdoba, Spain

3 Department of Applied Physics, University of Cordoba, Ed- C2, Campus de Rabanales, 14071 Córdoba, Spain

and chemical processes at low gas temperatures, and their low power consumption, are properties that make them very attractive from an applied point of view. It is well known that the reactivity of these plasmas comes from their high energy electrons, while the ions and neutral species retain a gas temperature (or heavy particle temperature) T_g relatively cold.

The development of well-controlled sources, able to maintain atmospheric plasmas with gas temperatures below 313 K (40 °C) and commonly known as cold atmospheric plasmas (CAPs) [1–3] or biologically tolerant plasmas (BTPs) [4], has brought the use of plasmas closer to the biomedicine field [1, 5, 6]. In this way, progress in the design of CAPs has fueled the so called plasma biomedicine technology.

Hand in hand with CAP source advances, research progressively focuses on the exploitation of mild plasma effects, with a challenge on the horizon: to achieve gradable, specific, and selective plasma effects on living cells through controlled interactions of specific plasma components with specific structural elements and functionalities of those living cells [6]. The action mechanisms of cold plasmas on cells are far from being well understood. Most likely, CAPs key to success is the ability of plasmas to produce active species at a tissue compatible gas temperature, allowing the intensification of traditional chemical and biochemical processes and a successful stimulation of new reactions [7].

Cold plasma is also a useful technology for sterilization and/or decontamination, due to the enormous potential derived from its high efficiency, its low gas temperature, and its ability to produce an interesting mixture of active species with antimicrobial activity. Plasma sterilization was patented by Menashi [8]. In the last couple of decades, a large amount of scientific contributions focused on plasma-based sterilization and decontamination of bacteria, spores, fungi, and biofilms [9]. Some of the reactive oxygen and nitrogen species (RONS) generated through the plasma action, such as O_3 and the radicals NO, H_2O_2, excited singlet O_2 and OH (depending on the type of gases used), have direct impact on microorganisms and contribute to the microbiocidal effects [7, 9]. The damage to bacterial cells is caused by the oxidation of unsaturated fatty acids in the cell membrane lipids, the oxidation of some aminoacids, and DNA damage (reviewed by Laroussi [10]). The physiological functions or pathways used by cells during oxidative and nitrosative stress are not fully understood. However, some functions have been identified suggesting that most of the metabolic pathways in the cell are altered by these stresses [11].

The integrity of the cell membrane is indispensable to sustain life. Any damage to the cell membrane may result in an osmotic imbalance, an altered permeabilization, a disrupted proton gradient, and a loss of function of the transport systems that may lead to cell lysis and death. Oxidative damage to membranes can arise through either lipid or membrane protein damage. Among biomolecules, lipids are the most sensitive molecules to oxidative stress. HOO·, and $O_2·^-$ radicals, singlet oxygen, and O_3 can initiate peroxidation of unsaturated fatty acids in the cell membrane and launch a peroxidation chain reaction. It is likely that the lipid peroxidation chain reaction begins after hydrogen abstraction from an unsaturated fatty acid to form a lipid radical. The lipid radical reacts with molecular oxygen to form a lipid peroxy radical (ROO′). This radical will attack another unsaturated fatty acid to form a fatty acid hydroperoxide (ROOH) perpetuating the initial reaction. Also, lipid alkoxy radicals can undergo cleavage of C–C bonds to form unsaturated fatty acid aldehydes and alkyl radicals. The peroxidation of lipids thus generates products which are shorter than the initial fatty acid [11].

As for protein damage, interactions between oxygen radicals and proteins lead to conversion of the aminoacids proline and arginine into carbonyl derivatives. Oxidative attack of histidinyl and prolyl residues converts them into asperginyl and glutamyl

derivatives, respectively. Methionine and cysteinyl residues are oxidized to form methionine sulfoxide derivatives and disulfide derivatives, respectively. These alterations inactivate enzymes and can lead to their degradation [11].

ROS can also induce oxidation and damage in DNA through reaction with sugars and bases. Oxygen radicals cause DNA damage in vitro and in vivo, and DNA repair-deficient mutants are hypersensitive to oxidative stress. Therefore, it is not surprising that oxidative stress leads to mutagenesis [11].

RONS also cause strong oxidative and nitrosative effects inside the cell. The cellular targets of NO and RNS (metalloproteins, thiols, glutathione and homocysteine) may serve as signal transducers, sensing NO and RNS, and resulting in altered gene expression and synthesis of protective enzymes [12].

Microbial growth can be controlled by chemical, physical or biological approaches. However, biofilms demonstrate unusual resistance to conventional sterilization methods compared to free-living, planktonic cells (reviewed in [13]). Biofilms are microbial communities encased in a protective matrix composed of polysaccharides, nucleic acids, and proteins. Bacterial biofilms are more resilient to typical sterilization/decontamination methods used for free-living, planktonic cells. Therefore, alternative methods are needed to eradicate these biofilms. The use of cold plasmas represents an excellent alternative to common sterilization methods since plasmas contain a mixture of reactive agents (free radicals, charged particles, UV photons, etc.) proven effective in the destruction of individual, planktonic microorganisms.

Dielectric barrier discharges (DBDs) are commonly used for non-thermal plasma generation (including CAPs). In this type of discharges there is at least one solid dielectric barrier (typically, glass, silica, ceramics, enamel, mica, or polymeric material) covering one of the two discharge electrodes, which acts as a ballast limiting the averaged current density in the gas space. Symmetric configurations with planar or cylindrical geometry are the most common configurations for DBDs, although the adaptation of DBDs to different problems has led to several novel configurations [14]. The discharge gap is typically in the range of 0.1–10 mm, and can be generated in ambient air or in gases flowing through this gap. Because of the capacitive character of the discharge, alternating or pulsed high voltages (1–100 kV_{rms}) are required for DBD operation, and frequencies ranging from 50 Hz to about 10 MHz are normally preferred, as at very high frequencies the current limitation by the dielectric becomes less effective. Plasmas generated in DBDs have electron temperatures considerably higher than the temperature of the ions and neutrals (which sometimes is as low as room temperature), therefore being of non-thermal nature. This type of plasma has proven to be well suited for disinfection or sterilization processes and enables the treatment of thermosensitive materials and living tissue that cannot undergo autoclaving.

We have previously demonstrated the usefulness of a helium/nitrogen plasma jet to eradicate *Pseudomonas aeruginosa* or *Chromobacterium violaceum* biofilms [15–20]. More recently, we used a coaxial DBD air-based plasma source for *P. aeruginosa* biofilm eradication. The DBD air-based plasma source was proven effective for *Pseudomonas* biofilm inactivation and it has the advantage of being affordable as it does not rely on expensive gases; and easy to handle for indirect surface treatment. Experiments were carried out with a discharge generated either in ambient air or in moistened air flow of 1 L/min. After 15 minutes of plasma treatment, biofilms were eradicated (measured as a decrease in culturable cells) for both treatment conditions resulting in a CFU/mL decrease of 5.6 $\log_{10}$ units (> 99.999%). For plasma generated in ambient air, a CFU/mL decrease of 1.6 $\log_{10}$ units was determined for a 3 minutes exposure; whereas a decrease of 2.7 $\log_{10}$

units was determined for the same plasma exposure time using moistened air. A good parameter to assess plasma removal efficiency is the decimal reduction time (D-value), the time required to reduce an original concentration of microorganisms by 90%. For the plasma generated in moistened air, the survival curve shows a double-slope kinetics with a D_1 of 1.14 ± 0.28 min for short exposure times, and a D_2 of 4.36 ± 0.63 min for longer exposure times. Taken together, these results demonstrate that moistened air inactivates biofilms more rapidly and efficiently than ambient air [21]. The better performance of a discharge generated in moistened air was attributed to the putative presence of RONS.

Aiming at understanding results by Soler-Arango et al. and eventually finding the best experimental conditions that could potentially result in better biofilm eradication; we characterized the air-based DBD plasma source recently designed. The characterization was carried out by optical emission spectroscopy (OES) techniques. These are non-invasive and easy-to-implement techniques that allow observing the plasma in real-time while determining its temperatures. Different compositions of the feed gas (air with different degrees of moisture and air/argon mixtures), gas flow rates, and applied voltages were studied. We also identified the active excited species in the plasma and gained a basic insight into the excitation processes in this kind of DBD plasma at atmospheric pressure, which is of great significance as these processes will eventually determine the formation of active species at the afterglow region in contact with the biofilm. All the OES measurements will be useful in future modeling of this device. As most of the radiation emitted by this plasma source falls in the ultraviolet region, the relative importance of UV radiation on biofilm inactivation was also analyzed.

Experimental Section

Plasma Generation

A detailed description of a DBD reactor operating at open atmosphere may be found elsewhere [21]. Figure 1a shows a schematic of this plasma source. It has a cylindrical (coaxial) geometry and a double dielectric barrier configuration. The inner electrode consists of a 1 mm-diameter iron wire inside a 6 mm-external diameter glass capillary tube sealed at the tip. The outer electrode is a 25 mm-long aluminum tape attached to a 1 mm-thick acrylic 10 mm-diameter tube. The discharge is powered through the inner electrode by two commercial transformers for neon signs (10 kV, 75 mA, 50 Hz), with their primary coils connected in parallel and their secondary ones in series, giving a maximum voltage of 20 kV. The operating voltage amplitude was controlled by means of a variable auto-transformer (Variac). The outer electrode was grounded. This plasma reactor allowed for the generation of plasmas under different experimental conditions (e.g., type of gas, gas flow rate, voltage).

We have previously shown that an air-based DBD plasma source represents an affordable but still convenient option for biofilm eradication [21]. For this reason, in this work we have mainly focused our study on plasmas generated in air as a major component of the feed gas. The discharge was generated in air with different relative moisture levels: ambient (without gas flow), "dry" (which means non-humidified but still drier than ambient air as the pumping air used for its injection into the system removed some moisture), and moistened air. Air was moistened by passing it through a humidifier filled
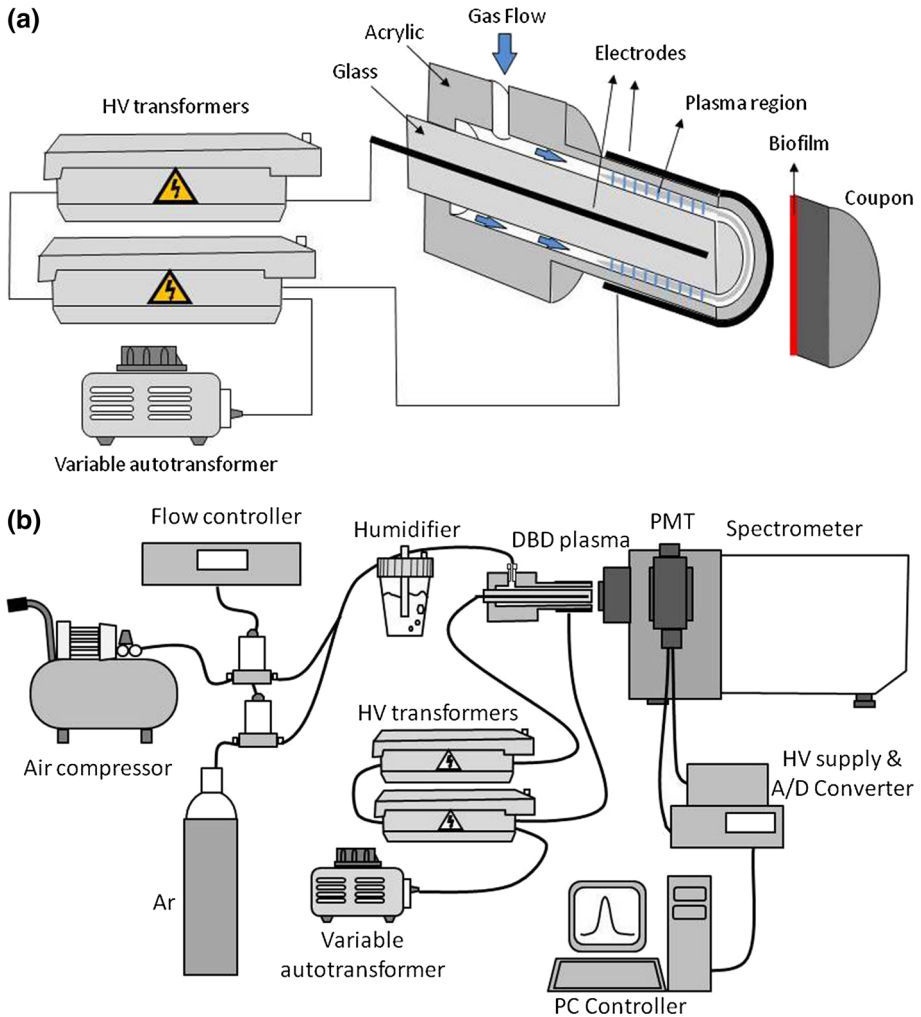
Fig. 1 **a** Schematic of the DBD plasma source. **b** Experimental set-up

with water and the air flow was determined using a commercial flow meter. Humidity was determined with an analog hygrometer (Luft48HIG-DH) for each condition.

For a better understanding of the excitation capacity of this DBD plasma source, plasmas generated in air/argon mixtures and pure argon were also studied. The rationale behind these experiments was to find appropriate gas combinations that would lead to an increased amount of reactive agents which in turn, could potentially result in better biofilm eradication. On the other hand, plasmas generated with different gas flow rates (1, 2, and 3 L/min) and different voltages (16 and 20 kV) were also studied.

As described in our previous work, in all the cases where air was used for plasma generation, the electric discharge took place at the interelectrode region and consisted of a series of short-lived filamentary micro-discharges [21]. Typical waveforms of current and voltage applied to the inner electrode during the discharge showed the filamentary

character of the discharge and also the existence of current peaks in the order of 10 mA with a negligible displacement current of ~ 0.01 mA superimposed.

OES Measurements

Figure 1b schematically depicts the experimental setup used to acquire the OES measurements. Light emission from the plasma was analyzed by using a Czerny-Turner type spectrometer (THR-1000S Jobin-Ivon) of 1 m focal length equipped with a 1200 grooves/mm holographic grating. Two different photomultipliers were used as detectors (Hamamatsu 212 and Hamamatsu R636-10) in order to cover the spectral interval from 200 to 900 mm. The spectra were recorded with different resolutions ranging from 0.028 to 0.11 nm.

Under all the conditions tested, the light emitted by the plasma was extremely weak. Therefore, to enable spectra recording, the plasma device was placed at the entrance slit of the spectrophotometer to collect most of the light released.

OES techniques allowed the determination of the excited species in the plasma and their relative population densities in arbitrary units, as well as the plasma gas temperature, and variations of these averaged plasma parameters depending on the type of feed gas, the gas flow rate, and the voltages used for its generation. The lack of emission of atomic hydrogen Balmer series lines precluded electron density determination.

Gas Temperature Determination of the Effluent Gas

The temperature of the effluent gas right outside the reactor was measured with an infrared thermal imaging camera (FLIR I7). For plasma technology to be used in biological applications or with thermosensitive samples it is important to keep the gas temperature below 40 °C to prevent damage of the material.

Ozone Measurement in the Effluent Gas

The measurement of the amount of ozone in the effluent gas was based on the ability of ozone to oxidize KI to I_2 in a neutral medium.

$$O_3 + 2I^- + 2H^+ \rightarrow I_2 + O_2 + H_2O \tag{1}$$

$$I_2 + I^- \rightarrow I_3^- \tag{2}$$
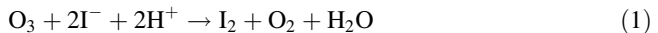
The effluent was circulated through an absorbent solution containing KI (6.8 g of KH_2PO_4, 7.1 g of Na_2HPO_4 and 5 g of KI in 500 mL of distilled water), where O_3 was trapped. Next, the amount of I_3^- was measured by UV–visible absorption spectroscopy. The concentration of I_3^- in the solution was determined from the maximum absorption at 352 nm, which was also used for the calibration curve. The calibration curve representing absorbance versus ozone concentration in µg/mL was previously determined considering a 1:1 O_3/I_3^- stoichiometry.

Qualitative Determination of Hydrogen Peroxide, Nitrate, and Nitrite in the Effluent

Qualitative measurements of hydrogen peroxide (H_2O_2), nitrate (NO_3^-), and nitrite (NO_2^-) generated in the plasma reactor were carried out with Peroxide (0.5–25 mg/L Mquant, Merck) and Nitrate/Nitrite (Macherey–Nagel) test strips. The strips were placed for one minute 4 mm away from the reactor outlet (the same distance plasma-sample used in [21]).

Results and Discussion

Plasma Excited Species

Dependency on Feed Gas Composition

Air-Based Plasmas Figure 2 shows typical spectra emitted from 200 to 940 nm by plasmas generated in air (20 kV) under different moisture conditions (i.e. moistened air, ambient air, and dry air). The gas flow rate for moistened and dry air was 1 L/min. The inset on the right side of the figure depicts the expanded spectrum corresponding to emissions from 200 to 400 nm.

In all cases, the main emission is the one of the 2nd positive system of N_2, resulting from the radiative de-excitation of N_2 excited molecules from $C^3\Pi_u$ to $B^3\Pi_g$ states. A very weak emission of molecular ions N_2^+ (1st negative system) corresponding to transitions from $B^2\Sigma_u^+$ states to $X^2\Sigma_g^+$ states was also found for moistened air, showing the presence of excited ions in these plasmas. Neither oxygen atomic lines nor oxygen molecular bands were detected.

Table 1 summarizes the plasma excited species observed (band heads for each molecular band) in the emission spectra and the spectroscopic features of their emissions.
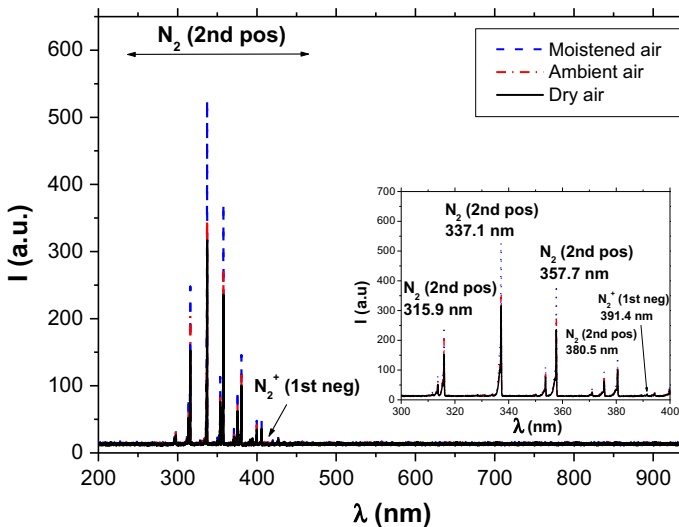

Fig. 2 Emission spectra of different air-based plasmas (F = 1 L/min, V = 20 kV)

Table 1 Spectroscopic features of species observed by OES in air plasmas [22]

Species	λ (nm)	Transition system band (v', v'')	E_{upper} (eV)	Species	λ (nm)	Transition system band (v', v'')	E_{upper} (eV)
N_2	295.3	$C^3\Pi_u \rightarrow B^3\Pi_g$ (4, 2)	12.02	N_2	375.5	$C^3\Pi_u \rightarrow B^3\Pi_g$ (1, 3)	11.33
	296.2	$C^3\Pi_u \rightarrow B^3\Pi_g$ (3, 1)	11.80		380.5	$C^3\Pi_u \rightarrow B^3\Pi_g$ (0, 2)	11.08
	297.7	$C^3\Pi_u \rightarrow B^3\Pi_g$ (2, 0)	11.57	N_2^+	391.4	$B^2\Sigma_u \rightarrow X^2\Sigma_g^+$ (0, 0)	18.9
	311.7	$C^3\Pi_u \rightarrow B^3\Pi_g$ (3, 2)	11.80	N_2	394.3	$C^3\Pi_u \rightarrow B^3\Pi_g$ (2, 5)	11.57
	313.6	$C^3\Pi_u \rightarrow B^3\Pi_g$ (2, 1)	11.57		399.8	$C^3\Pi_u \rightarrow B^3\Pi_g$ (1, 4)	11.33
	315.9	$C^3\Pi_u \rightarrow B^3\Pi_g$ (1, 0)	11.33		405.9	$C^3\Pi_u \rightarrow B^3\Pi_g$ (0, 3)	11.08
	337.1	$C^3\Pi_u \rightarrow B^3\Pi_g$ (0, 0)	11.08		420.1	$C^3\Pi_u \rightarrow B^3\Pi_g$ (2, 6)	11.57
	353.7	$C^3\Pi_u \rightarrow B^3\Pi_g$ (1, 2)	11.33		427.0	$C^3\Pi_u \rightarrow B^3\Pi_g$ (1, 5)	11.33
	357.7	$C^3\Pi_u \rightarrow B^3\Pi_g$ (0, 1)	11.08		434.4	$C^3\Pi_u \rightarrow B^3\Pi_g$ (0, 4)	11.08
	367.2	$C^3\Pi_u \rightarrow B^3\Pi_g$ (3, 5)	11.80		457.4	$C^3\Pi_u \rightarrow B^3\Pi_g$ (1, 6)	11.33
	371.1	$C^3\Pi_u \rightarrow B^3\Pi_g$ (2, 4)	11.57				

As shown with more detail in Fig. 3 for the most intense band of N_2 detected (band head at 337.1 nm), the highest amount of excited species was produced in moistened air-based discharges. This behavior is a consequence of the increase in the dielectrics surface conductivity caused by humidity, resulting in stronger micro-discharges [23]. Indeed, the relative humidity of the moistened airflow was $(80 \pm 5)\%$, $\sim (32 \pm 5)\%$ in the dry airflow, and $(39 \pm 5)\%$ in the ambient air.

Furthermore, emissions of the excited species OH and NO were not detected. According to Kogelschatz [23], the lack of detectable OH and NO species is typical in DBD plasmas generated in air with variable amounts of moisture, since in the presence of OH radicals, NO, and NO_2 are quickly transformed into HNO_2 and HNO_3, respectively.
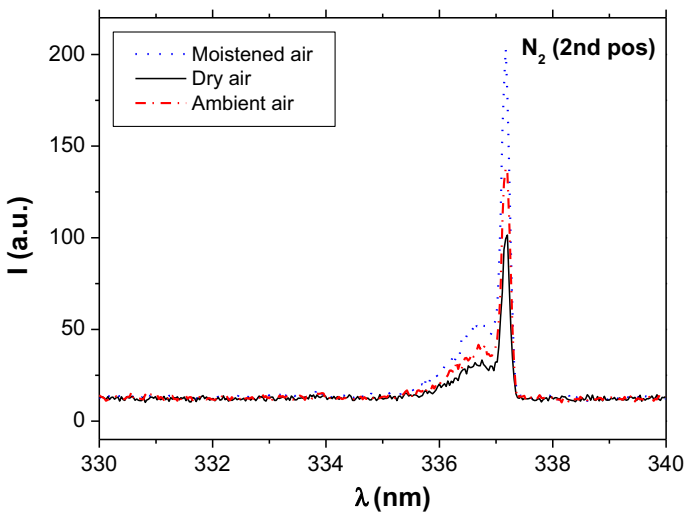
Fig. 3 N_2 (2nd positive system at 337.1 nm) emission spectra of different air-based plasmas (F = 1 L/min, V = 20 kV)

The almost exclusive presence of N_2 bands in the spectra and the absence of nitrogen excited atoms revealed that the energy of the discharge was mainly used for the excitation of nitrogen molecules ($\sim$ 11.1 eV), rather than in nitrogen dissociation. As shown later, these molecular excited species play a relevant role in ozone formation in this discharge.

Argon Plasmas Figure 4 shows the emission spectrum for the argon plasma generated under experimental conditions identical to those previously described for air-based plasmas (i.e. F = 1 L/min, V = 20 kV). The figure also depicts the spectrum obtained with 100% moistened air for comparison purposes.

The spectrum emitted by the argon plasma was characterized by a very strong emission of both the OH (3064 Å system) molecular band and Ar I (argon atomic) lines (corresponding to radiative de-excitation of $4p$ and $4p'$ excited states), and a moderate emission of the N_2 (2nd positive system) molecular bands. A very weak emission of O I lines was also detected in this case. The emission of the NH molecular band at 336.0 nm was found overlapped to the one of N_2 at 337.1 nm, but its very weak intensity precluded the identification of its band head. The presence in the spectrum of OH, N_2, NH and oxygen species accounts for the intake of ambient air into the open-to-the atmosphere discharge. Additionally, the bottle of argon feeding the discharge could also contain some water as impurities. Also, the presence of NH proved some N_2 dissociation in this argon discharge.

Table 2 gathers band heads and atomic lines identified in the argon plasma and their spectroscopic characteristics.

Figure 5 shows an expanded spectrum in the region between 305 and 320 nm for both argon and moistened air. It is clearly evident that only the argon plasma is able to generate a detectable amount of OH excited species.

Water dissociation in hydroxyl and hydrogen radicals through electron and argon metastable reactions is most likely the main mechanism of OH ($A^2\Sigma^+$) production [25].

$$H_2O\left(X^1A_1\right) + e^- \rightarrow H_2O\left(B^1A_1\right) + e^- \rightarrow OH\left(A^2\Sigma^+\right) + H + e^- \tag{3}$$
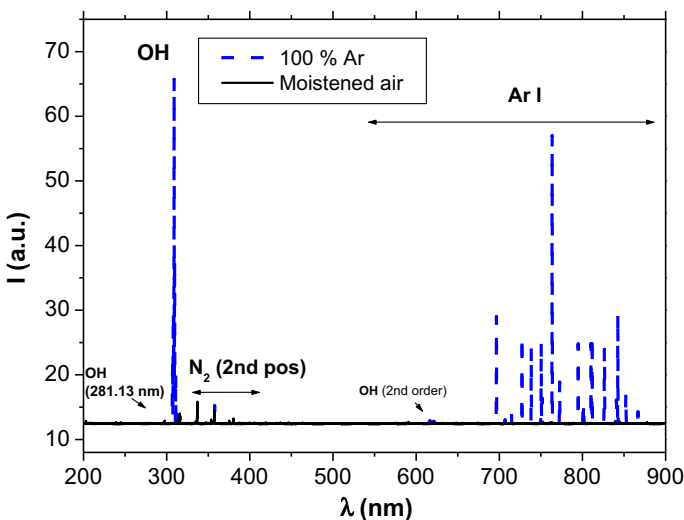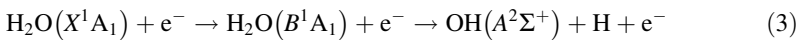

Fig. 4 Emission spectra for pure argon and moistened air plasma (F = 1 L/min, V = 20 kV)

Table 2 Spectroscopic features of species observed by OES in argon plasmas [22, 24]

Species	λ (nm)	Transition system band (v′, v′′)	E_{upper} (eV)	Species	λ (nm)	Transition upper level → lower level	E_{upper} (eV)
OH	281.1	$A^2\Sigma^+ \to X^2\Pi$ (1, 0)	4.43	Ar I	696.5	$3s^23p^5\,(^2P^\circ1/2)4p^2$ [1/2]1 → $3s^23p^5\,(^2P^\circ3/2)4s^2$ [3/2]°2	13.33
	308.9	$A^2\Sigma^+ \to X^2\Pi$ (0, 0)	4.03		706.7	$3s^23p^5\,(^2P^\circ1/2)4p^2$ [3/2]2 → $3s^23p^5\,(^2P^\circ3/2)4s^2$ [3/2]°2	13.30
NH	336.0	$A^3\Pi \to X^3\Sigma$ (0, 0)	3.4		714.7	$3s^23p^5\,(^2P^\circ1/2)4p^2$ [3/2]1 → $3s^23p^5\,(^2P^\circ3/2)4s^2$ [3/2]°2	13.28
N$_2$	295.3	$C^3\Pi_u \to B^3\Pi_g$ (4, 2)	12.02		727.3	$3s^23p^5\,(^2P^\circ1/2)4p^2$ [1/2]1 → $3s^23p^5\,(^2P^\circ3/2)4s^2$ [3/2]°1	13.33
	296.2	$C^3\Pi_u \to B^3\Pi_g$ (3, 1)	11.80		738.4	$3s^23p^5\,(^2P^\circ1/2)4p^2$ [3/2]2 → $3s^23p^5\,(^2P^\circ3/2)4s^2$ [3/2]°1	13.30
	297.7	$C^3\Pi_u \to B^3\Pi_g$ (2, 0)	11.57		750.4	$3s^23p^5\,(^2P^\circ1/2)4p^2$ [1/2]0 → $3s^23p^5\,(^2P^\circ1/2)4s^2$ [1/2]°1	13.48
	311.7	$C^3\Pi_u \to B^3\Pi_g$ (3, 2)	11.80		751.5	$3s^23p^5\,(^2P^\circ3/2)4p^2$ [1/2]0 → $3s^23p^5\,(^2P^\circ3/2)4s^2$ [3/2]°1	13.27
	313.6	$C^3\Pi_u \to B^3\Pi_g$ (2, 1)	11.57		763.5	$3s^23p^5\,(^2P^\circ3/2)4p^2$ [3/2]2 → $3s^23p^5\,(^2P^\circ3/2)4s^2$ [3/2]°2	13.17
	315.9	$C^3\Pi_u \to B^3\Pi_g$ (1, 0)	11.33		772.4	$3s^23p^5\,(^2P^\circ1/2)4p^2$ [1/2]1 → $3s^23p^5\,(^2P^\circ1/2)4s^2$ [1/2]°0	13.15
	337.1	$C^3\Pi_u \to B^3\Pi_g$ (0, 0)	11.08		794.8	$3s^23p^5\,(^2P^\circ1/2)4p^2$ [3/2]1 → $3s^23p^5\,(2P^\circ1/2)4s^2$ [1/2]° 0	13.28
	353.7	$C^3\Pi_u \to B^3\Pi_g$ (1, 2)	11.33		800.6	$3s^23p^5\,(^2P^\circ3/2)4p^2$ [3/2]2 → $3s^23p^5\,(^2P^\circ3/2)4s^2$ [3/2]°1	13.17
	357.7	$C^3\Pi_u \to B^3\Pi_g$ (0, 1)	11.08		801.5	$3s^23p^5\,(^2P^\circ3/2)4p^2$ [5/2]2 → $3s^23p^5\,(^2P^\circ3/2)4s^2$ [3/2]°2	13.10
	367.2	$C^3\Pi_u \to B^3\Pi_g$ (3, 5)	11.80		810.4	$3s^23p^5\,(^2P^\circ3/2)4p^2$ [3/2]1 → $3s^23p^5\,(^2P^\circ3/2)4s^2$ [3/2]°1	13.15
	371.1	$C^3\Pi_u \to B^3\Pi_g$ (2, 4)	11.57		811.5	$3s^23p^5\,(^2P^\circ3/2)4p^2$ [5/2]3 → $3s^23p^5\,(^2P^\circ3/2)4s^2$ [3/2]°2	13.08
	375.5	$C^3\Pi_u \to B^3\Pi_g$ (1, 3)	11.33		826.5	$3s^23p^5\,(^2P^\circ1/2)4p^2$ [1/2]1 → $3s^23p^5\,(^2P^\circ1/2)4s^2$ [1/2]°1	13.33
	380.5	$C^3\Pi_u \to B^3\Pi_g$ (0, 2)	11.08		840.8	$3s^23p^5\,(^2P^\circ1/2)4p^2$ [3/2]2 → $3s^23p^5\,(^2P^\circ1/2)4s^2$ [1/2]°1	13.30

Table 2 continued

Species	λ (nm)	Transition system band (v′, v″)	E_{upper} (eV)	Species	λ (nm)	Transition upper level → lower level	E_{upper} (eV)
	394.3	$C^3\Pi_u \rightarrow B^3\Pi_g$ (2, 5)	11.57		842.5	$3s^23p^5\ (^2P°3/2)4p^2\ [5/2]$ $2 \rightarrow 3s^23p^5\ (^2P°3/2)4s^2\ [3/2]°$ 1	13.10
	399.8	$C^3\Pi_u \rightarrow B^3\Pi_g$ (1, 4)	11.33		852.1	$3s^23p^5\ (^2P°1/2)4p^2\ [3/2]$ $1 \rightarrow 3s^23p^5\ (^2P°1/2)4s^2\ [1/2]°$ 1	13.28
	405.9	$C^3\Pi_u \rightarrow B^3\Pi_g$ (0, 3)	11.08		866.8	$3s^23p^5\ (^2P°3/2)4p^2\ [3/2]$ $1 \rightarrow 3s^23p^5\ (^2P°1/2)4s^2\ [1/2]°$ 0	13.15
	420.1	$C^3\Pi_u \rightarrow B^3\Pi_g$ (2, 6)	11.57	O I	777.2	$2s^22p^3\ (4S°)3p^5P\ 3 \rightarrow 2s^22p^3$ $(^4S°)3s^5S°\ 2$	10.74
	427.0	$C^3\Pi_u \rightarrow B^3\Pi_g$ (1, 5)	11.33		777.4	$2s^22p^3\ (4S°)3p^5P\ 2 \rightarrow 2s^22p^3$ $(4S°)3s^5S°\ 2$	10.74
	434.4	$C^3\Pi_u \rightarrow B^3\Pi_g$ (0, 4)	11.08		777.5	$2s^22p^3\ (4S°)3p^5P\ 1 \rightarrow 2s^22p^3$ $(4S°)3s^5S°\ 2$	10.74
	457.4	$C^3\Pi_u \rightarrow B^3\Pi_g$ (1, 6)	11.33		844.6	$2s^22p^3\ (4S°)3p^3P\ 2 \rightarrow 2s^22p^3$ $(4S°)3s^3S°\ 1$	10.99
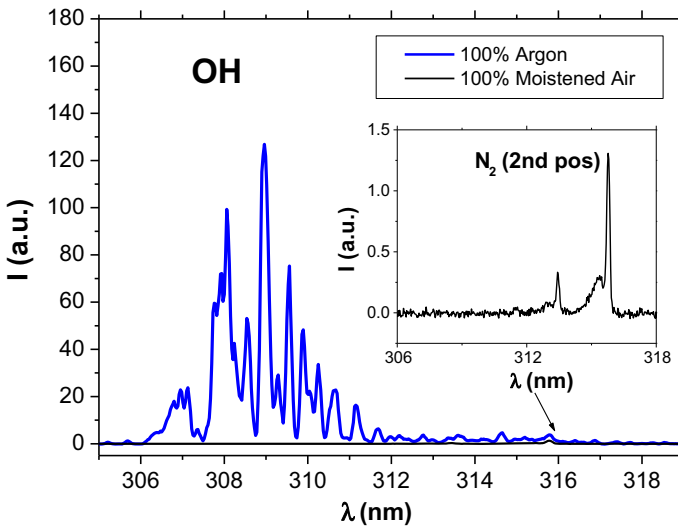
Fig. 5 Emission spectra for pure argon and moistened air plasma between 305 and 320 nm (F = 1 L/min, V = 20 kV)

$$H_2O(X^1A_1) + Ar^m \rightarrow OH(A^2\Sigma^+) + H + Ar$$
$$(E_{threshold} \sim 10 \text{ eV})$$

(4)
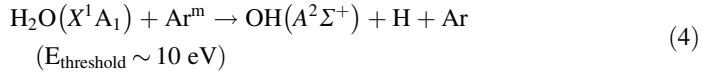
Spectra also show a higher excitation in argon plasmas when compared to air-based ones. Figure 6 shows the emission of N_2 band at 337.1 nm.

Generally, the higher excitation shown in this discharge can be attributed to the fact that argon micro-discharges in DBD devices are easier to create than air ones as the breakdown voltage is lower for the argon plasma. On the other hand, the energy transfer from argon metastable atoms also contributes to intensify the emission of N_2 molecules in $C^3\Pi_u$ states, as discussed later.

Air/Argon Plasmas Mixtures containing 5, 10, 20, 50, and 80% of air in argon were spectroscopically evaluated for the generation of excited species in plasmas. Figure 7 represents the evolution of normalized OH and N_2 band peaks (at 308.9 and 337.1 nm, respectively), and Ar I 810.4 nm line intensities with the percentage of air in the gas feeding the discharge for a total flow rate 1 L/min and 20 kV. The emission of the NH molecular band overlapped to the N_2 at 337.1 nm one, was detected in plasmas with air contents under 20%, but also in these cases the intensity of its band head could not be measured.

A progressive decrease of the OH band intensity takes place as the amount of air increases. For mixtures containing air exceeding 10%, OH was not detected. Interestingly, the excitation of OH bands follows the same trend as the excitation of argon atoms, suggesting that reaction (4) is most likely playing an important role in the generation of OH species in plasmas with high content of argon. A reduction in the amount of OH species in argon DBD plasma upon O_2 addition to the gas, has been measured by Sankaranarayanan et al. [26] using laser induced-fluorescence. The decrease in the amount of these species is attributed to an increased loss of electrons at higher oxygen concentration and to the destruction of OH by ozone through the following reaction [25, 26].
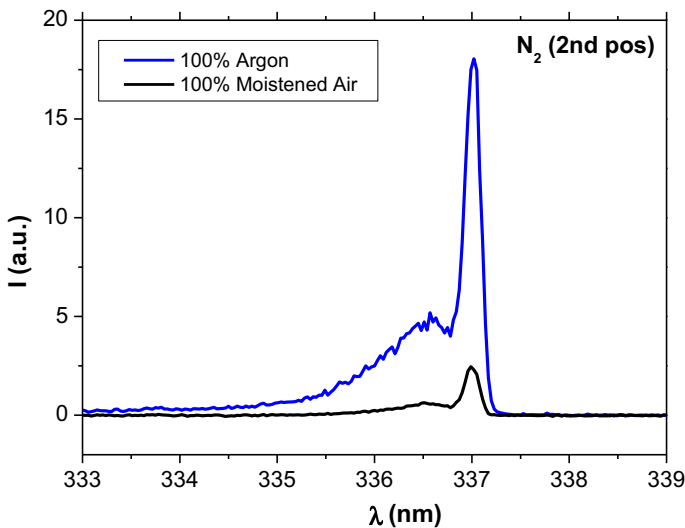

Fig. 6 N_2 (at 337.1 nm) emission spectra for pure argon and moistened air plasma between 305 and 320 nm (F = 1 L/min, V = 20 kV)
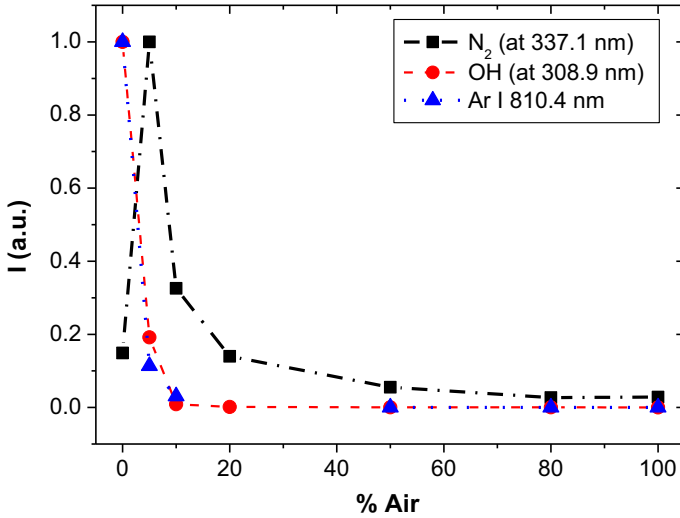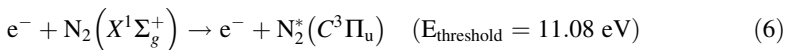
Fig. 7 Normalized OH and N_2 band heads and 810.4 nm argon atomic line intensities versus percentage of air in the gas feeding the discharge (F_{total} = 1 L/min, V = 20 kV)

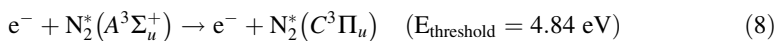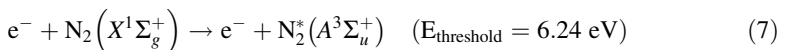$$OH + O_3 \rightarrow HO_2 + O_2 \qquad (5)$$

The quenching of OH ($A^2\Sigma^+$) excited states by collisions with molecular gases is an additional mechanism leading to the reduction of the emission of OH ($A^2\Sigma^+ \rightarrow X^2\Pi$) band upon the introduction of air in the plasma [27]. At atmospheric pressure, the lifetime of OH ($A^2\Sigma^+$) states in nitrogen is in the order of several nanoseconds and in water vapor it is below 1 ns. By contrast, the quenching of these states by argon atoms is very inefficient, as lifetime of OH ($A^2\Sigma^+$) in argon is almost radiative ($\sim$ 700 ns). This quenching mechanism, unlike others above mentioned, only reduces the OH ($A^2\Sigma^+ \rightarrow X^2\Pi$) emission intensity, not affecting the total density of OH in the plasma.

Nitrogen band emission had a different dependency on the amount of air in the mixture. On one hand, at very low air content the intensity of these bands increased with the percentage of air in the mixture. The higher intensities were measured for mixtures containing 5% of air. For higher air amounts, the intensity gradually decreased.

In plasmas generated in this DBD reactor open to the atmosphere, the excitation of nitrogen molecules to $C^3\Pi_u$ state is likely produced from electron collisions with nitrogen molecules at ground state $X^1\Sigma_g^+$, through direct excitation

$$e^- + N_2\left(X^1\Sigma_g^+\right) \rightarrow e^- + N_2^*\left(C^3\Pi_u\right) \quad (E_{threshold} = 11.08 \text{ eV}) \qquad (6)$$

or step-wise processes

$$e^- + N_2\left(X^1\Sigma_g^+\right) \rightarrow e^- + N_2^*\left(A^3\Sigma_u^+\right) \quad (E_{threshold} = 6.24 \text{ eV}) \qquad (7)$$

$$e^- + N_2^*\left(A^3\Sigma_u^+\right) \rightarrow e^- + N_2^*\left(C^3\Pi_u\right) \quad (E_{threshold} = 4.84 \text{ eV}) \qquad (8)$$

These molecules subsequently de-excites to $B^3\Pi_g$ level, causing the emission of the 2nd positive system of N_2 observed

$$N_2\left(C^3\Pi_u\right) \rightarrow N_2\left(B^3\Pi_g\right) + h\nu \quad \text{(2nd pos.)} \tag{9}$$
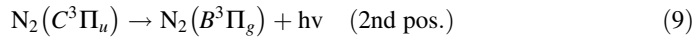
In cases where plasma is generated using argon with moderate air contents (including 100% argon plasmas, as they are in contact with air), argon metastable atoms (E ∼ 11.5–11.8 eV) also play a relevant role in the excitation of nitrogen molecules, through excitation transfer reactions with the ground state of molecular nitrogen, N_2 $(X^1\Sigma_g^+)$ [25, 28–30]:

$$Ar^* + N_2\left(X^1\Sigma_g^+\right) \rightarrow Ar^0 + N_2^*\left(C^3\Pi_u\right) \tag{10}$$
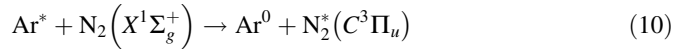
This mechanism partly accounts for the intensification of the N_2 $(C^3\Pi_u \rightarrow B^3\Pi_g)$ band emission observed in argon plasmas compared to air-based ones (see Fig. 6). With increasing air and N_2 contents in the discharge, the amount of N_2 $(C^3\Pi_u)$ excited molecules also increases. The higher dissociation of nitrogen molecules taking place in plasmas with a higher content of argon (detected through formation of NH species) would also help to explain the decrease of the emission of N_2 bands observed upon a moderate reduction of the argon content.

On the other hand, as the amount of air increases in the discharge, the population of argon excited atoms progressively quenches (Fig. 7), thus reducing at the same time their contribution to the excitation of nitrogen molecules. This fact explains why, for air proportions over 5%, the intensity of N_2 bands decreases even though the amount of N_2 becomes higher.

Dependency on the Gas Flow Rate

The gas flow rate also determines the amount of excited species generated by this cold plasma reactor. Figure 8 shows the dependency of the nitrogen molecule excitation on the flow rate in air based plasmas.

Trends observed for plasmas generated in moistened or dry air are different. In the case of moistened air, a flow rate increase leads to an increase in the dielectrics surface conductivity caused by a higher humidity, which results in strongest micro-discharges and thus, in an enhanced excitation. On the contrary, higher flow rates in dry air cause the opposite effect because of the drying of the dielectrics surface.

Figure 9 shows the change in the species excitation with the gas flow rate in argon plasmas. An increase in argon flow rate favors the excitation of argon atoms and hydroxyl radicals, at least in the range of the flow rates studied. In argon plasmas there is a higher amount of argon and its impurities (including water) when using higher argon flow rates. Moreover, because these plasmas are created in open atmosphere, there is some air intake into them. At a higher argon flow rate, the air fraction in the gas reduces and thus, a lower quenching of OH $(A^2\Sigma^+)$ states takes place, enhancing OH $(A^2\Sigma^+ \rightarrow X^2\Pi)$ emission. The decrease of the intensity of N_2 bands observed in this case (with a higher argon fraction), could be indicative of a higher dissociation of nitrogen molecules.

Dependency on the Voltage

The voltage applied to the discharge also allows controlling species excitation in this reactor. Two boundary conditions were considered: the highest voltage feasible for the electrical system (determined by the transformers and VARIAC), and the lowest one
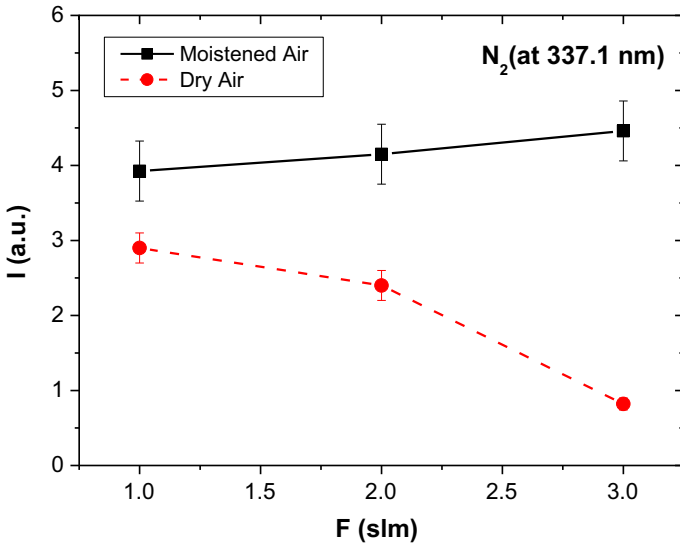
Fig. 8 Intensity of the N₂ band peak at 337.1 nm versus gas flow rate of air with different moisture content (V = 20 kV)
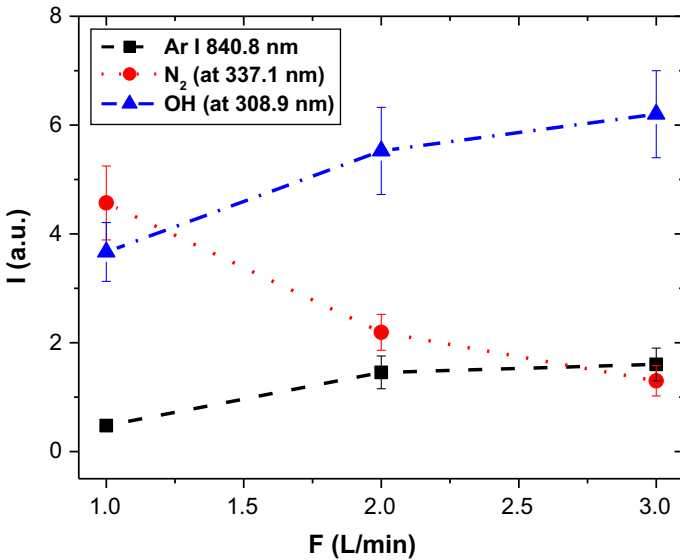

Fig. 9 Variations of OH and N₂ band intensities and 810.4 nm argon atomic line intensities with the gas flow rate (V = 20 kV)

allowing light detection. Figure 10 shows the amount of excited species versus voltage. Again, the excitation is enhanced by the moisture content of the discharge at high and low voltages.

Plasma Temperatures

Gas Temperature

In all the cases studied, spectra present emission bands or atomic lines allowing the determination of the plasma gas temperature.

As N_2 ($C^3\Pi_u$) excited molecules are present in all plasmas and conditions tested, gas temperatures (T_g) were determined from the rotational temperature obtained from the analysis of the N_2 ($C^3\Pi_u \rightarrow B^3\Pi_g$) ro-vibrational spectra. MassiveOES software recently developed by Voráč and Synek at CEPLANT Center in Brno has been used for simulations of N_2 bands [31, 32]. N_2 band with head at 315.9 nm was used for this purpose. Also, simulations with MassiveOES software made possible the identification of the already mentioned NH band at 336.0 nm.

In cases where the plasma spectrum depicted a strong enough Ar I 810.4 nm line, additional measurements were performed from the collisional broadening of the line by using the method recently developed by Rodero and García [33]. In this way, the no self-absorbed profile of the line experimentally measured, was approximated by Voigt shaped profile with a full with at half maximum (FWHM) W_V given by

$$W_V \approx \frac{W_L}{2} + \sqrt{\left(\frac{W_L}{2}\right)^2 + W_G^2} \tag{11}$$

where W_L and W_G are the FWHM of the Lorentzian and Gaussian parts of the profile, respectively. The Lorentzian profile was mainly determined by van der Waals and resonance collisional broadenings (with FWHMs W_W and W_R, respectively)
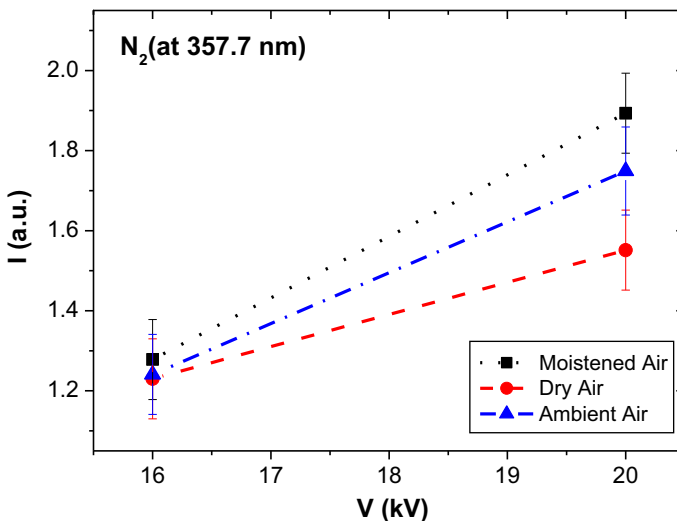

Fig. 10 N_2 band intensity (at 357.7 nm) versus voltage applied for different air plasmas (F = 1 L/min)

Table 3 Gas temperatures of different air-based plasmas (V = 20 kV) derived from simulations of N_2 band at 315.9 nm

	1 L/min	2 L/min	3 L/min
T_g (dry air) (K)	310 ± 10	315 ± 10	320 ± 11
T_g (moistened air)(K)	324 ± 10	319 ± 7	307 ± 8
T_g (ambient air) (K)	320 ± 11		

$$W_L(T_g) = W_C(T_g) \approx W_W(T_g) + W_R(T_g) = \chi_{Ar} \underbrace{\frac{1.825}{T_g^{0.7}} + \chi_{Air} \frac{5.312}{T_g^{0.7}}}_{W_W} + \underbrace{\chi_{Ar} \frac{15.546}{T_g}}_{W_R} \quad (12)$$

being χ_{Ar} and χ_{Air} the molar fraction of argon and air in the discharge. For more details the reader is referred to [33].

On the other hand, the Gaussian part of the profile was attributed to the instrumental broadening

$$W_G(T_g) \approx W_I \quad (13)$$

By measuring W_V and knowing the value of the instrumental broadening, W_L was derived. Finally, the gas temperature can be determined from Eq. (12).

Table 3 gathers the values of T_g measured in the different air-based plasmas generated in dry or moistened air, with a voltage of 20 kV and gas flow rates of 1, 2, and 3 L/min. Temperatures never exceed 335 K (including error) remaining approximately constant, within the margin of error. It should be kept in mind that these are averaged temperatures at the interelectrode region inside the plasma reactor, which could differ from the temperature of the gas effluent.

Table 4 summarizes the temperatures T_g measured in plasmas with different dry air/ argon amounts at 20 kV and a gas flow rate of 1 L/min. The higher temperature corresponds to the pure argon plasma. The addition of a small fraction of air produces a moderate reduction in the gas temperature, which reaches its lowest value for a 100% of air.

Finally, Table 5 shows the values of T_g measured for two different applied voltages, in air-based plasmas. Again, temperatures always kept under 335 K, remaining approximately constant within the margin of error.

IR Temperatures

Gas temperatures at the reactor outlet were measured under different experimental conditions using an IR camera. The end of the inner electrode right outside was used as the target. This temperature could be likely considered as an estimation of the gas effluent temperature, assuming efficient thermalization between this gas and the inner electrode. Neither voltage nor percentage of moisture in the gas feeding the discharge causes significant variations on the temperature of the effluent (see Table 6). A slightly higher temperature is measured when the discharge is operated with argon.

In summary, air-based plasmas have the lower gas and effluent temperatures, thus being useful for thermosensitive materials and biomedical applications.

Table 4 Gas temperatures of different (dry) air/argon plasmas

Air fraction (%)	$T_{g, N2}$ (K)	$T_{g, Ar I}$ (K)	$T_{g, OH}$ (K)
0	365 ± 24	Selfabs.	355 ± 6
5	323 ± 12	330 ± 5	–
10	319 ± 9	325 ± 5	–
20	318 ± 9	320 ± 7	–
25	318 ± 10	315 ± 8	–
50	317 ± 9	–	–
80	318 ± 12	–	–
100	310 ± 8	–	–

Table 5 Gas temperatures of different air-based plasmas (F = 1 L/min) derived from simulations of N_2 band at 315.9 nm

	16 kV	20 kV
T_g (dry air) (K)	300 ± 18	310 ± 8
T_g (moistened air)(K)	320 ± 15	324 ± 10
T_g (ambient air) (K)	321 ± 24	320 ± 11

Table 6 IR temperatures under different voltage conditions (F = 1 L/min)

	16 kV	20 kV
T_{effl} (dry air) (K)	300	300
T_{effl} (moistened air) (K)	230	301
T_{effl} (ambient air) (K)	299	300
T_{effl} (argon) (K)	303	302

Oxidizing Species Generated by the Plasma Reactor

It is well known that one of the most important applications of DBDs is ozone generation. The amount of ozone produced per unit of time by the reactor operated in moistened air was determined following the method described in 2.4. An amount of 1.8 ± 0.4 µg/min of O_3 was measured.

The ozone generation process in this air-based discharge (also open to the air) can be explained by a sequence of reactions involving oxygen molecules [23]. First, the dissociation of O_2 molecules (dissociation energy ~ 5.2 eV) produces oxygen atoms O, through intermediate reactions of excitation by electron collisions of the O_2 from the ground state to $A^3\Sigma_u^+$ (6 eV) or $B^3\Sigma_u^-$ (8.4 eV) excited states.

$$O_2 + e^- \rightarrow O_2^* + e^- \rightarrow O + O + e^- \tag{14}$$
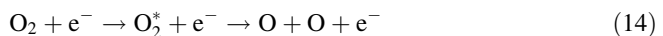
Subsequent three body reactions involving O and O_2 lead to the formation of ozone.
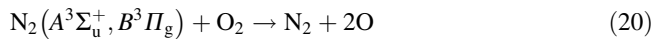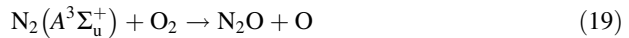
$$O + O_2 + M \rightarrow O_3 + M \tag{15}$$

where M is a third collision partner that in the case of air could be O, O_2, O_3 or, most likely N_2.

Moreover, in these air-based plasmas, the energy of electrons is also used in the excitation of N_2 molecules (~ 9.8 eV) and their subsequent dissociation

$$N_2 + e^- \rightarrow N_2^* + e^- \rightarrow N + N + e^- \qquad (16)$$

Additional reaction paths involving nitrogen atoms and the excited molecular states N_2 $(A^3\Sigma_u^+)$ and N_2 $(B^3\Pi_g)$, can produce extra oxygen atoms for ozone generation [23]:

$$N + O_2 \rightarrow NO + O \qquad (17)$$

$$N + NO \rightarrow N_2 + O \qquad (18)$$

$$N_2\left(A^3\Sigma_u^+\right) + O_2 \rightarrow N_2O + O \qquad (19)$$

$$N_2\left(A^3\Sigma_u^+, B^3\Pi_g\right) + O_2 \rightarrow N_2 + 2O \qquad (20)$$

As pointed out by Kogelschatz, about half of the ozone produced in air discharges results from these indirect processes. This is the reason why ozone formation in air discharges takes much longer than in oxygen, and a considerable fraction of the energy initially lost by electrons in collisions with nitrogen molecules can be recovered through reactions (17)–(20) for ozone generation. Thus, the higher the amount of excited nitrogen molecules in the discharge, the higher the amount of ozone generated, which would lead to a better efficacy of the reactor in biofilm eradication. We have already shown that in air-based plasmas generated in the DBD reactor, N_2 excitation is increased by the amount of moisture and the voltage applied. Therefore, N_2 excitation is the highest for moistened air, intermediate in ambient air and the lowest in dry air.

On the other hand, qualitative measurements of H_2O_2, NO_3^- and NO_2^- species generated in the discharge were carried out using appropriate strips. H_2O_2 species were detected in all the plasmas tested. However, NO_2^- species were not detected under any circumstance. Finally, NO_3^- was only detected in experiments using moistened and dry air.

Biofilm Growth and Plasma Treatment

Pseudomonas aeruginosa biofilms were grown on stainless-steel 316 L 12.7-mm diameter coupons and treated with plasma for various exposure times as described elsewhere [21]. Biofilms were then scraped off the coupons, suspended, serially diluted, and plated in duplicates. Plates were incubated at 37 °C (310 K) and evaluated for colony-forming-units (CFU) formation by counting the colonies.

To study the effect of UV radiation on biofilm inactivation, a 3 cm diameter and 2.5 mm thick piece of quartz was mounted between the discharge and the coupon, 4 mm away from the biofilm. The quartz prevented all the reactive agents besides UV photons to reach the sample. Experiments were carried out as indicated above and survival curves (log CFU/mL vs exposure time) constructed.

Figure 11 depicts the survival curves for *P. aeruginosa* biofilms grown in the above-mentioned conditions and treated with plasma operating in a moistened air flow of 1 L/min (red curve) or with a quartz window interposed between the plasma afterglow and the sample (blue curve). The latter is equivalent to a UV treatment since the quartz window blocks the other reactive agents in the plasma from reaching the biofilm.
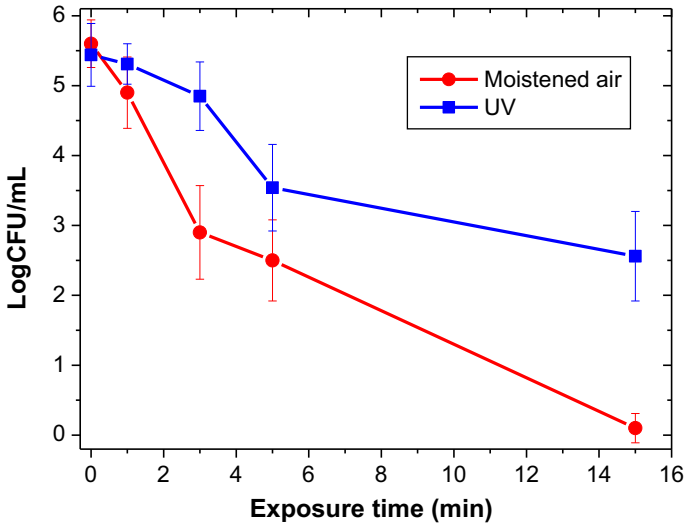
Fig. 11 Survival curve: log of the number of CFU/mL versus plasma exposure time. *P. aeruginosa* biofilms grown in continuous culture on stainless-steel coupons in AB synthetic medium were treated with DBD plasma generated in ambient air (red curve) or with UV (blue curve). Results are the average of four independent experiments. Each experiment was performed in duplicates. Error bars represent the standard error of the mean (Color figure online)

The graphs show that *P. aeruginosa* biofilms were completely eradicated after a 15-min treatment with plasma in moistened resulting in a CFU/mL decrease of 5.6 $\log_{10}$ units (> 99.999% killing efficacy). In the case of the interposed quartz window, the decrease in CFU/mL was 2.9 $\log_{10}$ units and therefore a 47.06% killing efficacy was obtained. These results demonstrate that for this DBD plasma source, UV contribution is considerable and UV photons play an important role in plasma-mediated biofilm inactivation.

Concluding Remarks

In summary, in this work we have assessed various different experimental conditions resulting in a diversity of plasma species depending on the composition of the feed gas.

In a previous contribution, we determined that moistened air inactivates biofilms more rapidly and efficiently than ambient air [21]. Here we determined that under those conditions the main emission corresponds to the one of the second positive system of N_2 and neither oxygen atomic lines nor oxygen molecular bands were detected. The almost exclusive presence of N_2 bands in the spectra and the absence of nitrogen excited atoms revealed that the energy of the discharge was mainly used for the excitation of the vibrational and rotational levels of nitrogen molecules, rather than in nitrogen dissociation or excitation of other species. These molecular excited species play a relevant role in ozone formation in this discharge. Emissions of excited species OH and NO were not detected which is typical in DBD plasmas generated in air with variable amounts of moisture, since the presence of OH radicals, NO, and NO_2 are quickly transformed into HNO_2 and HNO_3. Although NO and OH were not detected in our DBD plasma device as they were with the plasma jet operating in helium/nitrogen [15], the DBD plasma device efficiently and

rapidly eradicated *P. aeruginosa* biofilms. The fact of not detecting more reactive RONS in the spectra does not imply that those species are not produced by the reactor. OES techniques allowed us to detect only excited reagent species in the plasma itself (where excitation was high enough), not accounting for non-excited (ground state) ones. In addition, the presence of ozone, hydrogen peroxide, and nitrate in the afterglow indicates that a relatively complex plasma chemistry involving relatively long lifetime radicals takes place at this region of this discharge, resulting in the formation of active species undetectable by OES [24]. We believe that some of those species are contributing to biofilm eradication.

In addition, in air-based plasmas excited N_2 molecules are involved in reactions paths leading to enhance ozone generation. As ozone plays a role in biofilm eradication, understanding the excitation of N_2 molecules in order to increase ozone generation, might result in an improved tool for biofilm removal.

Nevertheless, we determined that argon plasmas alone or with the contribution of some air, depicted a very strong emission of OH which is known to be very reactive in terms of its biological activity. A progressive decrease of the OH band intensity took place as the amount of air increased. For mixtures containing air exceeding 10%, OH was not detected. Taken together, these results show the potentiality of argon/air based plasmas to produce a reactive environment which in turn, would oxidize biofilm biomolecules. We expect to test these different argon/air combinations to eradicate *P. aeruginosa* biofilms in an efficient and timely manner. Knowledge gained through these experiments, would set up the basis for better strategies for bacterial biofilm inactivation.

References

1. Weltmann KD, von Woedtke T (2016) Plasma Phys Control Fusion 59:014031
2. Gay-Mimbrera J, García MC, Isla-Tejera B, Rodero-Serrano A, Vélez García-Nieto A, Ruano J (2016) Adv Ther 33:894–909
3. Stoffels E, Roks AJM, Deelman LE (2008) Plasma Process Polym 5:599–605
4. Barekzi N, Laroussi M (2013) Plasma Process Polym 10:1039–1050
5. Fridman G, Friedman G, Gutsol A, Shekhter AB, Vasilets VN, Fridman A (2008) Plasma Process Polym 5:503–533
6. von Woedtke Th, Reuter S, Masur K, Weltmann KD (2013) Phys Rep 530:291–320
7. Graves DB (2012) J Phys D Appl Phys 18:263001
8. Menashi WP (1968) US Patent 3.383.163
9. Moisan M, Barbeau J, Moreau S, Pelletier J, Tabrizian M, Yahia LH (2001) Int J Pharm 226:1–21
10. Laroussi M (2002) IEEE Trans Plasma Sci 30:1409–1415
11. Farr SB, Kogoma T (1991) Microbiol Rev 55:561–585
12. Poole RK (2005) Biochem Soc Trans 33:176–180
13. Brelles-Mariño G (2012) J Bioprocess Biotech 2:4
14. Brandenburg R (2017) Plasma Sources Sci Technol 26:053001
15. Abramzon N, Joaquin JC, Bray JD, Brelles-Mariño G (2006) IEEE Trans Plasma Sci 34:1304–1309

16. Becker K, Koutsospyros A, Yin SM, Christodoulatos C, Abramzon N, Joaquin JC, Brelles-Mariño G (2005) Plasma Phys Control Fusion 47:B513–B523
17. Joaquin J, Kwan C, Abramzon N, Vandervoort K, Brelles-Mariño G (2009) Microbiology 17:724–732
18. Zelaya A, Stough G, Rad N, Vandervoort K, Brelles-Mariño G (2010) IEEE Trans Plasma Sci 38:3398–3403
19. Zelaya A, Vandervoort K, Brelles-Mariño G (2012) In: Machala Z, Hensel K, Akishev Y (eds) Plasma for bio-decontamination, medicine and food security. NATO science for peace and security series A. Springer, Dordrecht **(Chapter 11)**
20. Vandervoort KG, Brelles-Mariño G (2014) PLoS ONE 9:e108512
21. Soler-Arango J, Xaubet M, Giuliani L, Grondona D, Brelles-Mariño G (2017) Plasma Med 7:43–63
22. Pearse RWB, Gaydon AG (1963) The identification of molecular spectra, 3rd edn. Wiley, Hoboken
23. Kogelschatz U (2003) Plasma Chem Plasma Process 23:1–46
24. Kramida A, Ralchenko Y, Reader J (2016) NIST ASD Team NIST Atomic Spectra Database (version 5.4) (Online). National Institute of Standards and Technology, Gaithersburg, MD. http://physics.nist.gov/asd. Accessed 12 Jan 2017
25. Lu X, Naidis GV, Laroussi M, Reuter S, Graves DB, Ostrikov K (2016) Phys Rep 630:1–84
26. Sankaranarayanan R, Pashaie B, Dhali SK (2000) Appl Phys Lett 77:2970–2972
27. Li L, Nikiforov A, Xiong Q, Britun N, Snyders R, Lu X, Leys C (2013) Phys Plasmas 20:093502
28. Yu QS, Yasuda HK (1998) Plasma Chem Plasma Process 18:461–485
29. Britun N, Gaillard M, Ricard A, Kim YM, Kim KS, Han JG (2007) J Phys D Appl Phys 40:1022–1029
30. García MC, Varo M, Martínez P (2010) Plasma Chem Plasma Process 3:241–255
31. Voráč J, Synek P, Potočňáková L, Hnilica J, Kudrle V (2017) Plasma Sources Sci Technol 26:025010
32. Voráč J, Synek P, Procházka V, Hoder T (2017) J Phys D Appl Phys 50:294002
33. Rodero A, García MC (2017) J Quant Spectrosc Radiat Transf 198:93–103